RESEARCH ARTICLE

BON VIEW PUBLISHING

High Coupling Efficiency Silicon-Based Colloidal Quantum Dot Electroluminescent Devices with Ag Reflectors

Jiajun Zhu[1], Yuxuan Ye[1], Fankai Zheng[2,3], Yilan Zhang[1], Zhiyang Lu[1], Hechun Zhang[1], Sifan Chen[1], Jiongwen Fang[1], Yunji Yi[4,*], Kai Wang[2,3,*] and Dan Wu[1,*]

[1]College of New Materials and New Energies, Shenzhen Technology University, China

[2]Institute of Nanoscience and Applications, Southern University of Science and Technology, China

[3]Department of Electronic and Electrical Engineering, Southern University of Science and Technology, China

[4]College of Integrated Circuits and Optoelectronic Chips, Shenzhen Technology University, China

Abstract: On-chip silicon photonic chips are critical in various applications including chip-to-chip communication, sensing, and near-eye display technologies, but they all face significant challenges in efficiently coupling light sources onto the chip. This study introduces a design adopting colloidal quantum dot light-emitting diode (QLED) as an on-chip light source coupled with optimized Ag reflectors below and within the SiN waveguide. The inclined Ag reflector was positioned directly below the QLED within the GaN waveguide with an optimal angle of 45° and 100 nm thickness, along with a planar Ag reflector 500 nm below the waveguide with 200 nm thickness. Numerical simulation results indicate that at a distance of 50 μm from the QLED center, the average coupling efficiency of the device is 9.76%, which is 2.58 times higher than the counterpart without the Ag reflector. These findings demonstrate a significant improvement in coupling efficiency, suggesting a promising approach for future on-chip light source designs.

Keywords: quantum dots electroluminescent device, waveguide coupling efficiency, on-chip light sources

1. Introduction

As the electronic integrated circuit sizes approach physical limits and the need for communication networks grows rapidly, photonic integrated circuits (PICs) are gaining attention as an indispensable technology due to their unique advantages of expandability, openness, low delay, and lower energy use per transmitted bit [1]. The PICs have two main types [2]: one based on the III–V semiconductor platform [3, 4] and the other based on the silicon platform [5–8]. However, adopting pure III–V-based PICs usually restricts the foundry to small wafers [9]; silicon photonics has been the main choice due to compact size [10, 11], compatibility with current complementary metal-oxide-semiconductor technology [12–14], and the ability to be widely integrated in electronic products [15–17].

Leveraging the advantages of silicon photonics, numerous passive and active photonic elements have been effectively realized on the silicon photonics platform. However, as an indirect bandgap material, silicon restricts its light-emission efficiency. III–V-based lasers are considered one of the most practical and efficient on-chip laser sources in silicon photonics to date. Typical integration approaches include bonding-based heterogeneous integration [18, 19] and direct epitaxial growing [20]. In bonding-based heterogeneous integration, the light generated in the III–V material is evanescently coupled into the silicon waveguides, avoiding issues related to lattice mismatch. However, this approach has limitations such as high costs and limited scalability for mass production [21]. The primary challenge with direct heteroepitaxial growth is the high density of threading dislocations caused by the large lattice mismatch between III and V materials and silicon. In recent years, colloidal quantum dot light-emitting diode (QLED) as the basic building block for future laser designs has attracted more and more attention due to its excellent photoelectric properties, such as tunable electroluminescent wavelength, high photoluminescence efficiency, solution processability, and low cost [22–27]. Recently, significant progress has been made in the integration of QLED with silicon photonic platforms, demonstrating their potential as on-chip light sources. For instance, QLED emitting layers have been successfully integrated onto silicon substrates using spin casting, showcasing the feasibility of direct integration of QLED with silicon photonics [28]. In another approach, micro-contact printing

*Corresponding authors: Yunji Yi, College of Integrated Circuits and Optoelectronic Chips, Shenzhen Technology University, China. Email: yiyunji@sztu.edu.cn; Kai Wang, Institute of Nanoscience and Applications and Department of Electronic and Electrical Engineering, Southern University of Science and Technology, China. Email: wangk@sustech.edu.cn; Dan Wu, College of New Materials and New Energies, Shenzhen Technology University, China. Email: wudan@sztu.edu.cn

was employed to create patterned QD films, enabling multicolor QLED structures with high spatial resolution and demonstrating the versatility of QLED in silicon-based devices [29]. Moreover, QLEDs have been integrated with silicon nitride (SiN) waveguides, achieving direct coupling and further validating their potential for compact, efficient, and scalable photonic circuits. Specifically, by positioning the CdSe/CdS QLED device within the evanescent field of a low-loss SiN single-mode waveguide, electroluminescent waveguide coupling is achieved. This design offers several notable advantages. First, the device can be fabricated as a post-process on existing SiN waveguide platforms, making it cost-effective and suitable for large-scale production. Additionally, the use of a low-loss ZnO electron transport layer (ETL) in contact with the waveguide reduces passive optical losses, allowing high optical gain even with a thin quantum dot layer, overcoming the limitations of traditional designs that require thicker quantum dot layers. This provides a solid technical foundation for future integrated photonics applications [30].

However, the use of CdSe/CdS QDs on silicon substrates as on-chip light sources directly coupled to SiN waveguides is in its infancy, and the average coupling efficiency of these devices is still limited; specifically, the output power of the QLED is limited by the poor average coupling efficiency (β_{avg} is 0.8%) [30]. This limitation arises because QDs are approximated as isotropic dipole emitters [31]; their random orientations within the device result in only a single dipole orientation effectively coupling to the fundamental waveguide mode. This leads to a coupling efficiency of less than 1% with the SiN single-mode waveguide, limiting the single-mode waveguide's output power to just 2 nW. Despite the limited waveguide coupling efficiencies, this waveguide-integrated electroluminescent device provides valuable insights for the design of on-chip QD light sources. Currently, most strategies for enhancing waveguide coupling efficiency rely on laser sources, including grating couplers [32, 33], cavity-based structures [34, 35], and reflector-assisted couplers [36]. However, there remains a lack of effective coupling enhancement schemes tailored to QLED-based emitters. Therefore, improving the coupling efficiency between QLED and silicon-based waveguides remains an important challenge in the development of practical, electrically driven photonic integrated systems.

In this work, a new silicon-substrate electroluminescent QLED design is proposed. The CdSe/CdS QLED is used as an on-chip light source, which is coupled with a SiN waveguide. To enhance the average coupling efficiency of the design, two types of Ag reflectors are separately introduced into two distinct regions. Specifically, one type of Ag reflector is placed below the SiN waveguide on the silicon substrate, acting as a reflective plane to redirect light that would otherwise escape downward into the SiO$_2$ layer back into the transmission path. The other type of Ag reflector is inclined and embedded within the SiN waveguide directly below the coupled light source, acting as a reflective plane to redirect light propagating in the opposite direction of the output energy back into the transmission path. Through desired simulation, it is found that the average coupling efficiency of the design with both Ag reflectors included ($\beta_{avg} = 9.76\%$) is about two times higher than that of the design without any Ag reflection structure ($\beta_{avg} = 3.78\%$). Specifically, when only the Ag planar reflector is included, the average coupling efficiency improves to $\beta_{avg} = 8.79\%$, while incorporating only the inclined Ag reflector achieves a slightly higher coupling efficiency of $\beta_{avg} = 9.39\%$. These results demonstrate that the combination of both reflectors

synergistically enhances the coupling efficiency, marking an important step toward constructing high-performance on-chip silicon photonic chips.

2. Materials and Methods

Figure 1(a) shows the basic structure of the design, Figure 1(b) shows the cross-section view of the basic design in the YZ plane, and Figure 1(c) shows the cross-section of the same design in the XZ plane. The design consists of silicon substrate/SiN on SiO$_2$/ZnO/(Ti/Au metal stack, comprising 20 nm Ti/100 nm Au/20 nm Ti)/(CdSe/CdS QDs)/4,4′,4″-Tri(9-carbazoyl) triphenylamine (TCTA)/N,N′-di (naph-thalen-1-yl)-N,N′-diphenylbenzidine (NPB)/1,4,5,8,9,11-hexaazatriphenylene-hexacarbonitrile (HAT-CN)/Al. The ZnO layer serves as both the ETL and the electron injection layer. The TCTA, NPB, and HAT-CN function as an optimized band-alignment layer, hole transport layer (HTL), and hole injection layer, respectively. The Ti/Au and Al metal contacts serve as the cathode and anode, respectively. The emitting layer uses CdSe/CdS QDs as the active layer material. This waveguide coupling design facilitates the injection of electrons from the Ti/Au cathode through the ZnO into the CdSe/CdS QDs layer, while simultaneously injecting holes from the Al anode through the organic HTLs. The electrons and holes recombine and emit light within the QD layer. The emitted light is then coupled into and guided by the SiN waveguide.

From the above analysis, it can be found that the transmission of light has two main loss paths, which can be seen from the red arrows in Figure 1(d). The first loss path can be seen that part of the light will escape through the waveguide to SiO$_2$. The second loss path can be seen that the light emitted by QDs will transport toward both ends of the waveguide after coupling into the waveguide. Assuming that the right end is the energy output end, the light transmitted in the opposite direction (left end) will be regarded as the loss of light energy.

Therefore, to increase the coupling efficiency, this study proposes a design as shown in Figure 1(e) and (f). For the first light loss path induced energy loss, an Ag planar reflector will be introduced below the waveguide, and the light transmitted into SiO$_2$ will be reflected back into the waveguide and continue to propagate along the waveguide. For the second light loss path, an inclined Ag reflector is introduced within the SiN waveguide directly below the QLED coupling to the waveguide on the silicon substrate, and the light transmitting in the opposite direction with respect to the output end will be reflected back to improve the coupled efficiency. The planar Ag reflector can be fabricated using well-established micro- and nanofabrication techniques such as magnetron sputtering [37], and the fabrication of the inclined Ag reflector is feasible and has been demonstrated in prior studies [38]. In this study, the average coupling efficiency β_{avg} was used to measure the optical energy output efficiency at the output end; the β_{avg} was defined as:

$$\beta_n = \frac{E_{out}}{E_{in}} \tag{1}$$

$$\beta_{avg} = \frac{\beta_{0°90°0°} + \beta_{0°90°90°} + \beta_{0°0°90°}}{3} \tag{2}$$

where β_n is the transmission efficiency of one dipole oscillation direction. Since QDs can be approximated as point dipole sources [39], optical simulations were conducted using the dipole model. The E_{in} denotes the total energy of light emitted by the QDs. E_{out}

Figure 1

The structures of the basic designs are shown: (a) overall schematic of the basic design, (b) the cross-section of the basic design at the central position in the (b) YZ plane view and (c) XZ plane view. The light loss path and the structure of the silicon-based SiN waveguide on-chip QLED are shown: (d) light loss paths schematic, the cross-section of Ag reflectors at the central position in the (e) YZ plane view and (f) XZ plane view
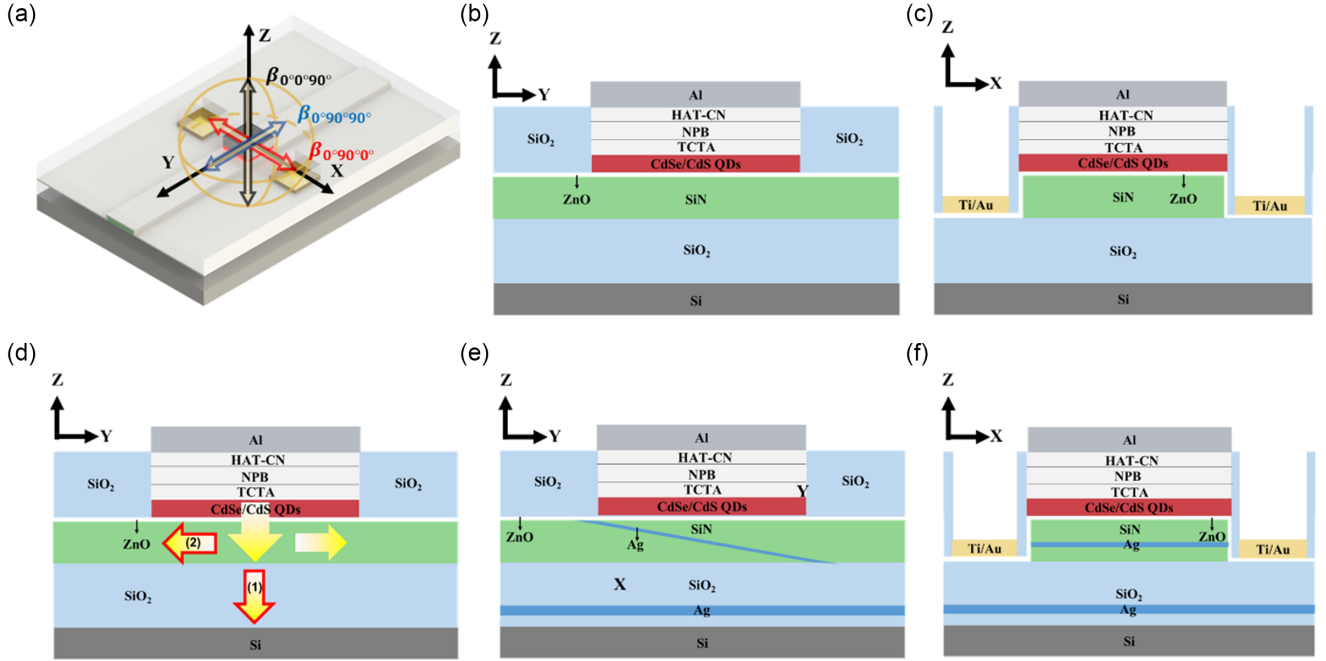
represents the light energy at the output port of the waveguide. The average coupling efficiency β_{avg} is defined as the mean transmission efficiency across three orthogonal dipole oscillation directions, specifically along the x, y, and z directions marked as $\beta_{(0°,90°,0°)}$, $\beta_{(0°,90°,90°)}$, and $\beta_{(0°,0°,90°)}$, respectively. To obtain the optimal parameters of the Ag reflectors to achieve the optimal waveguide coupling efficiency, four models were built and analyzed using Ansys Lumerical finite difference time domain (FDTD) solution software. The first model serves as the basic model without any reflectors. The second model adds an Ag planar reflector below the SiN waveguide. The third model incorporates an inclined Ag reflector within the waveguide. The fourth model combines both an Ag planar reflector and an inclined Ag reflector as shown in Figure 1(e)–(f).

3. Results and Analysis

3.1. Light coupling and transmission of QLED coupled with silicon-based SiN waveguide without Ag reflector

Figure 2(a)–(h) illustrates the electric field distributions at various cross-sections (XZ plane) along the SiN waveguide from Y = 1.07 μm to 1.95 μm. The field evolution indicates a typical multi-mode interference behavior induced by the superposition of guided modes with different propagation constants. This effect arises from the finite spectral bandwidth of the QLED source, which leads to the excitation of multiple guided modes with slightly different propagation constants, resulting in spatial oscillations and power redistribution during the light propagation process [40, 41]. As shown in Figure 2(i), although the majority

of the emitted light from the QLED is successfully coupled into the SiN waveguide, part of the energy leaks into the SiO$_2$ substrate due to the limited vertical confinement, constituting the primary out-of-plane loss pathway. Furthermore, Figure 2(j) demonstrates that, in the absence of end-reflectors or directional couplers, the coupled light propagates symmetrically toward both ends of the waveguide. Consequently, only the light transmitted toward the designated output end contributes to the effective signal, while the energy propagating in the opposite direction is inherently wasted. Figure 2(k) presents the transmission efficiencies corresponding to three orthogonal dipole oscillation directions, along with the averaged coupling efficiency β_{avg}. The transmission rate exhibits a rapid decline within the initial 10 μm, attributed to mode mismatch and substrate leakage loss, and then approaches a stable value along the waveguide. The β_{avg} of the basic design reaches 3.78% after 50 μm of propagation. These results indicate that the coupling and transmission performance are mainly limited by the substrate leakage loss, the multi-mode interference effect, and the absence of directional output structures. Therefore, introducing Ag reflectors is expected to substantially enhance the light coupling efficiency and waveguide transmission performance.

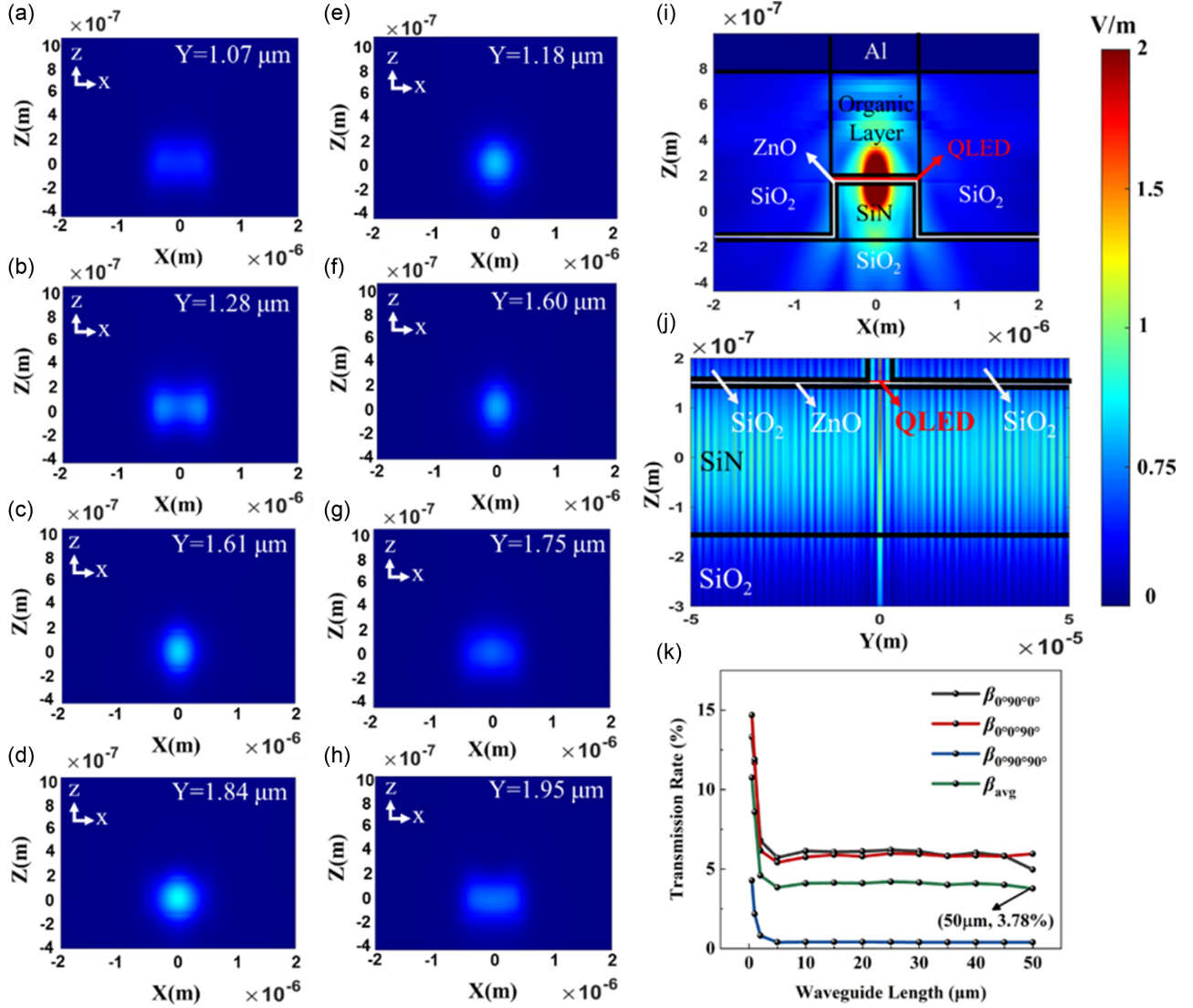### 3.2. Influence of an Ag planar reflector on light coupling and transmission of QLED coupled with silicon-based SiN waveguide

For the first energy loss path, this study proposes an Ag planar reflector below the waveguide, as shown in Figure 3(a), to reflect the light escaping to the SiO$_2$ substrate back into the SiN waveguide. In order to achieve the optimal transmission efficiency in the

Figure 2
Electronic field distribution without Ag reflectors design are shown: where (a) Y = 1.07 μm, (b) Y = 1.28 μm, (c) Y = 1.61 μm, (d) Y = 1.84 μm, (e) Y = 1.18 μm, (f) Y = 1.60 μm, (g) Y = 1.75 μm, and (h) Y = 1.95 μm. The cross-sectional optical field distribution of the design at the central position is shown in the (i) XZ plane and the (j) YZ plane. (k) The transmission efficiency and the average coupling efficiency of the basic design in the three dipole oscillation directions are shown
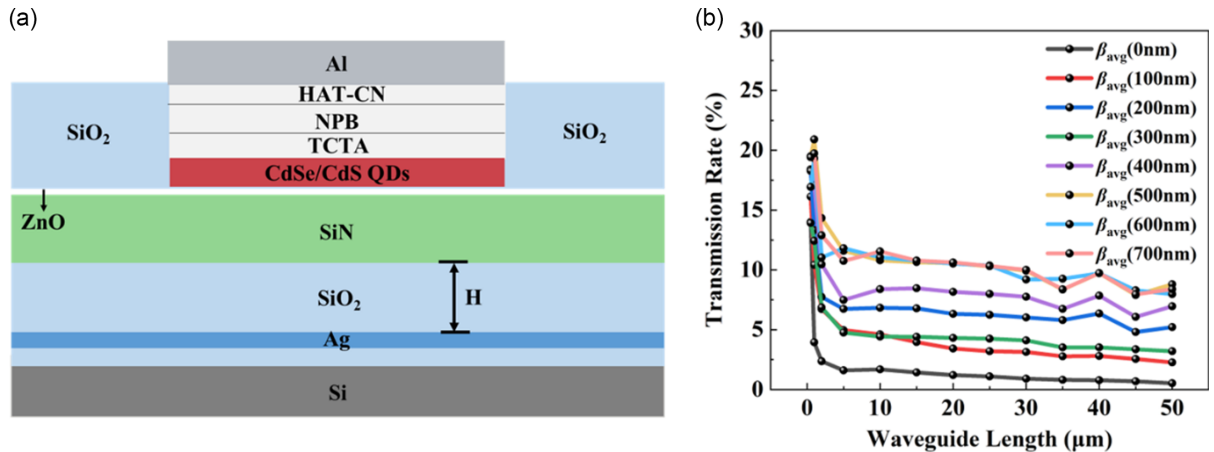

Figure 3
Schematic of an Ag planar reflector on light coupling and transmission of QLED coupled with a silicon-based SiN waveguide is shown: (a) the cross-section of the design at the central position in the YZ plane, (b) the average coupling efficiency of different Ag planar reflector positions relative to the lower surface of the waveguide

waveguide, the study investigates the distance H of the Ag planar reflector relative to the lower surface of the waveguide from 0 nm to 700 nm. As shown in Figure 3(b), the energy decreases exponentially at the center of the on-chip light source of the waveguide and tends to be stable after 5 μm. Through the simulation results, the average coupling efficiency at 50 μm from the waveguide center increases as the reflector distance increases from 0 nm to 500 nm and decreases as the reflector distance increases from 500 nm to 700 nm. Therefore, the optimal transmission efficiency is achieved when the reflector distance is 500 nm.

Figure 4(a)–(h) presents the electric field distributions across the XZ plane at various propagation distances (Y = 1.40 to 2.13 μm) along the SiN waveguide with a planar Ag reflector placed 500 nm beneath the lower surface. The field evolution illustrates mode interference and spatial power redistribution along the propagation axis. Although the transverse field patterns appear similar to those in the basic designs (Figure 2), enhanced vertical confinement is more clearly observed in the central cross-sectional distributions shown in Figure 4(i)–(j). Specifically, Figure 4(i) demonstrates that the Ag planar reflector effectively reflects the downward-leaking radiation into the SiO$_2$ substrate, redirecting it back toward the SiN waveguide. This reflection promotes field recapture into guided modes, resulting in stronger vertical confinement and reduced substrate losses. Figure 4(j) further confirms this effect, showing enhanced bidirectional guided wave propagation due to reflective recirculation. As shown in Figure 4(k), the transmission efficiency for dipoles oriented along X, Y, and Z directions stabilizes after approximately 5 μm of propagation. The average coupling efficiency β_{avg} reaches 8.79%

Figure 4
Electronic field distribution with an Ag planar reflector positioned at 500 nm from the lower surface of the waveguide of the QLED coupled with a silicon-based SiN waveguide is shown: where (a) Y = 1.40 μm, (b) Y = 1.52 μm, (c) Y = 1.60 μm, (d) Y = 1.75 μm, (e) Y = 1.81 μm, (f) Y = 1.89 μm, (g) Y = 2.00 μm, (h) Y = 2.13 μm. The cross-sectional energy distribution of the design at the central position is shown in the (i) XZ plane and in the (j) YZ plane. (k) The transmission efficiency and the average coupling efficiency of the basic design in the three dipole oscillation directions are shown
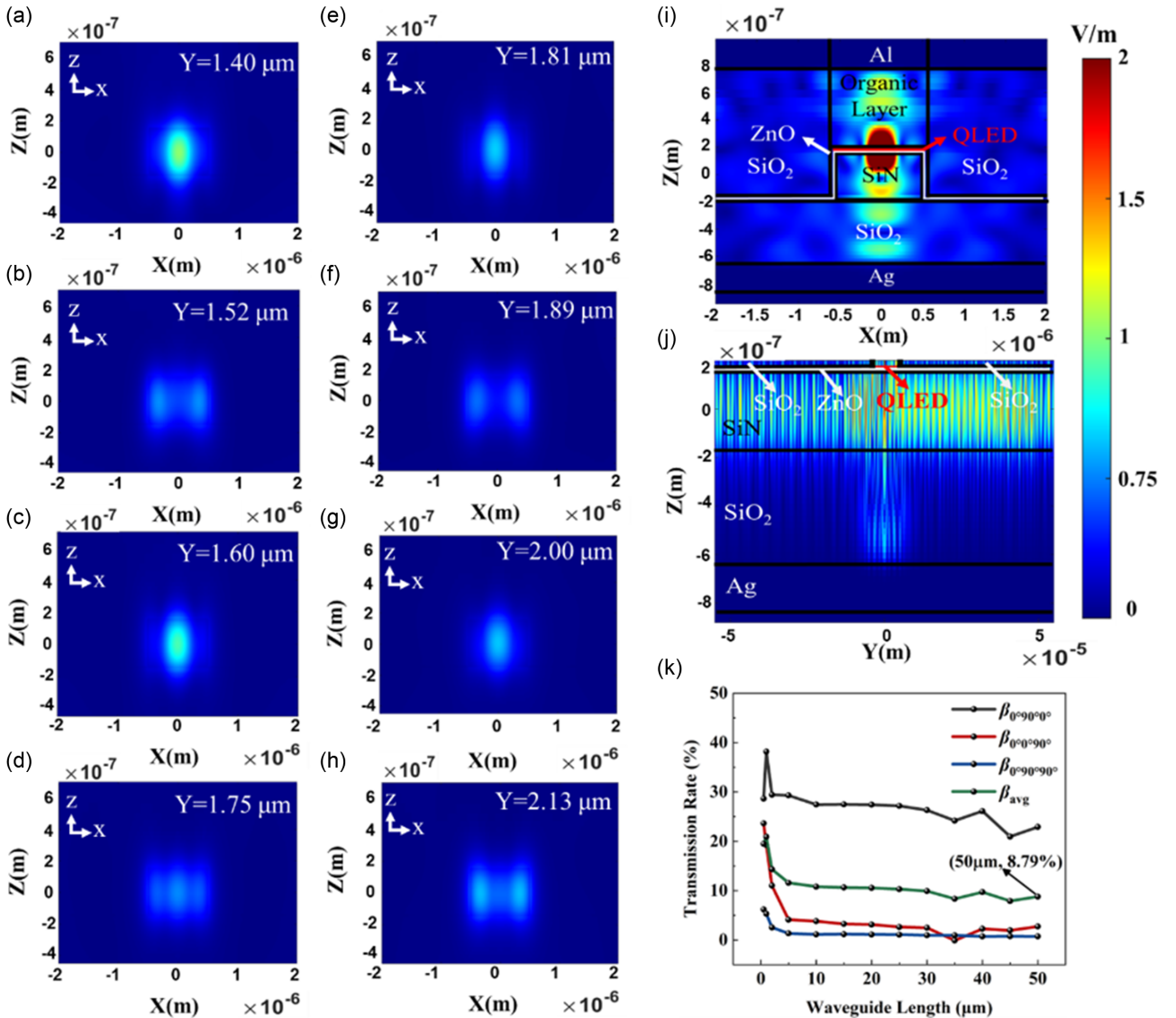
at 50 μm, representing a 2.32-fold improvement over the basic design $\beta_{avg} = 3.78\%$. These results highlight that the Ag reflector significantly suppresses out-of-plane leakage, leading to improved waveguide coupling performance.

3.3. Influence of an inclined Ag reflector on light coupling and transmission of QLED coupled with silicon-based SiN waveguide

An inclined Ag reflector is introduced within the SiN waveguide directly below the coupled light source, whose structure is shown in Figure 5(a) and (b), and the light transmitted in the opposite direction of the output energy is reflected back to improve the light outcoupled efficiency from the waveguide. In order to achieve the optimal results, the study investigates different Ag reflector inclination angles θ to study their influence on the average coupling efficiency of the design. Figure 5(c) shows the energy transfer efficiency as a function of the tilt angle of the Ag reflector where the three dipole oscillations of $\beta_{(0°,90°,90°)}$, $\beta_{(0°,90°,0°)}$, and $\beta_{(0°,0°,90°)}$ are separately studied. For each dipole oscillation direction, the maximal coupling efficiency can be achieved as 46°, 43°, and 73°, respectively. When the dipole oscillates in the direction of 0°90°0°, the transmission efficiency shows the highest level as about two to four times that of the other two directions (0°90°90° or 0°0°90°). To maximize the transmission efficiency across the three orthogonal dipole oscillation directions, the optimization step should be refined next

in the region where the reflector inclination is close to the transmission efficiency in the direction of 0°90°0°. Figure 5(d) shows the scan results of the reflector dip refinement step near the transmission efficiency extremum. The results show that the design exhibits the highest average coupling efficiency after oscillation stabilization when the Ag reflector angle is 45°. Therefore, the tilt angle is set to 45° as the optimization result of the gain structure, and it is applied to the design of the basic design.

Figure 6(a)–(h) presents the electric field distributions across the XZ plane at different propagation distances (Y = 1.46 to 12.12 μm) for the waveguide structure incorporating a 45° inclined Ag reflector. These field patterns reveal multi-mode interference during propagation. Unlike previous configurations, the inclined Ag reflector introduces directional reflection, favoring light propagation toward the right-side output port. As shown in Figure 6(i), the 45° Ag reflector redirects leftward-propagating light into the forward direction, promoting directional energy transfer. Figure 6(j) clearly illustrates that the light initially propagating in both directions is partially redirected from the left branch into the right-side waveguide by the inclined reflector, thereby improving output efficiency. Figure 6(k) shows the transmission efficiencies for three orthogonal dipole oscillation directions. The average coupling efficiency β_{avg} increases and stabilizes after approximately 10 μm of propagation, reaching 9.39% at 50 μm. This represents a 2.47-fold enhancement compared to the basic design. The results indicate that the 45° Ag reflector not only suppresses out-of-plane radiation loss but also

Figure 5

The structure and simulation results of the design that has the inclined Ag reflector are shown: the cross-section of the design at the central position in the (a) YZ plane and in the (b) XZ plane, (c) FDTD simulation results of the fine-step scan of the Ag reflector tilt angle, (d) the average coupling efficiency of the fine-step scan of the reflector tilt angle near the region of peak transmission efficiency
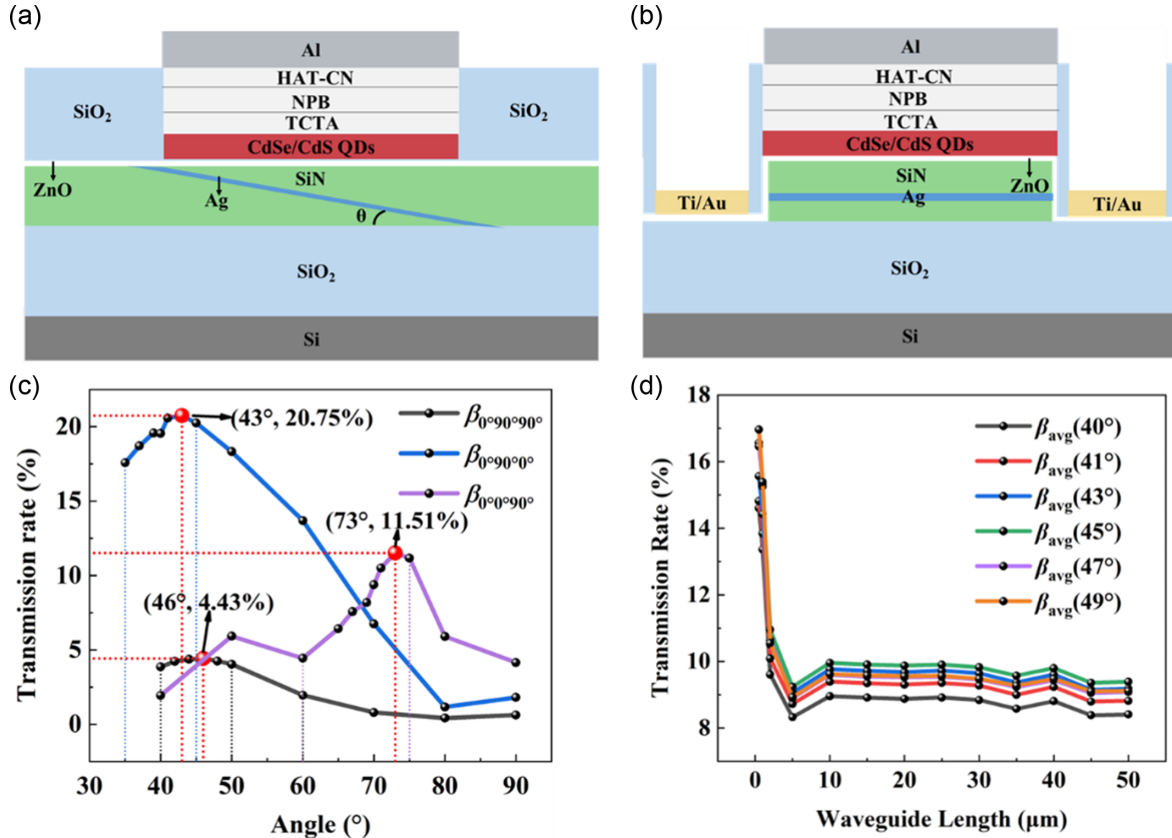
Figure 6

Electronic field distribution with a 45° inclined Ag reflector is shown: where (a) Y = 1.46 μm, (b) Y = 2.36 μm, (c) Y = 3.37 μm, (d) Y = 4.60 μm, (e) Y = 6.96 μm, (f) Y = 9.09 μm, (g) Y = 10.89 μm, (h) Y = 12.12 μm. (i) The cross-sectional energy distribution of the design at the central position is shown in the (j) XZ plane and in the (k) YZ plane. (k) The transmission efficiency and average coupling efficiency of the design with an inclination of 45° Ag reflector in the three dipole oscillation directions are shown
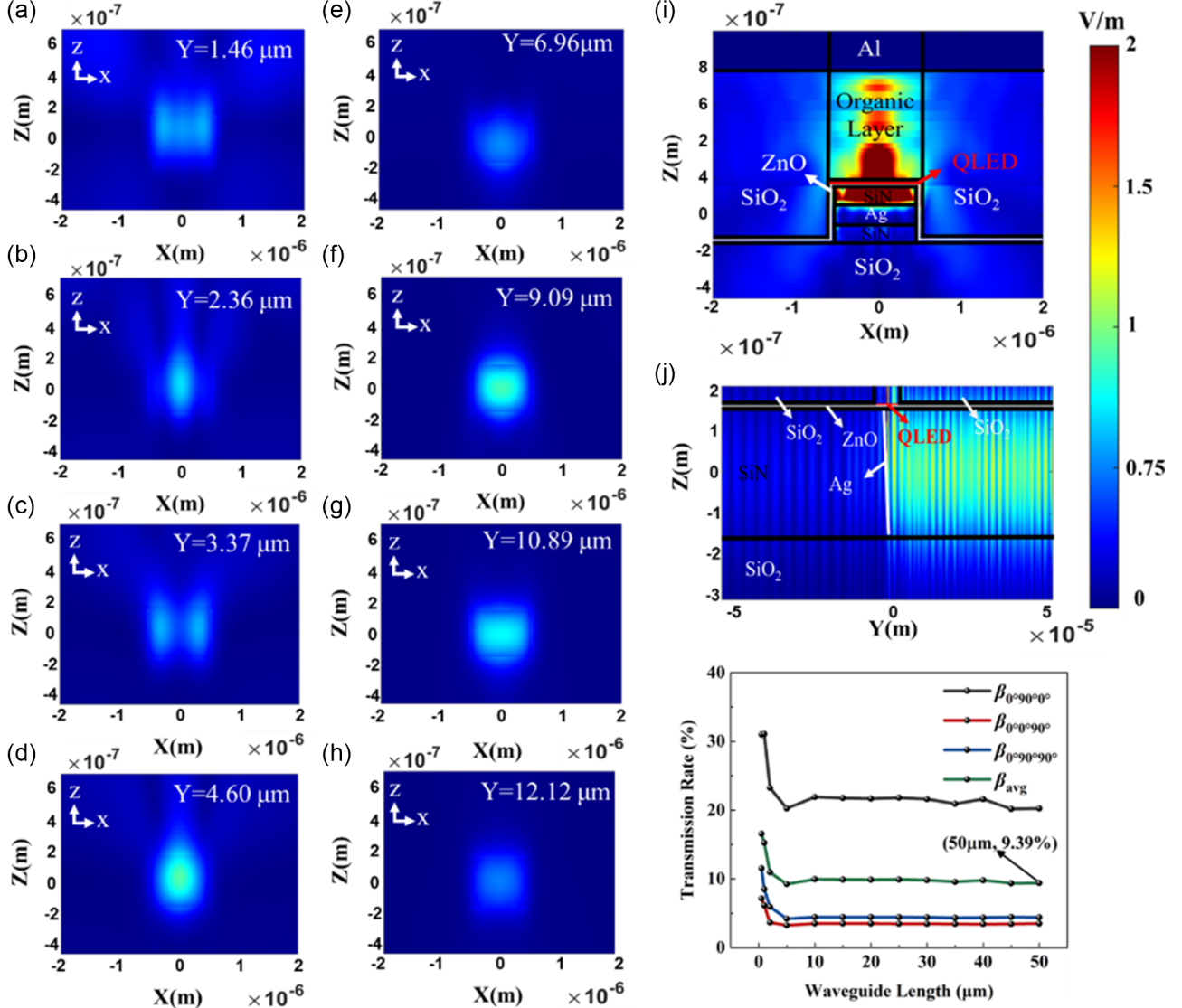
facilitates directional light redirection, significantly improving waveguide coupling and output efficiency.

3.4. Influence of both a planar and an inclined Ag reflector on light coupling and transmission of QLED coupled with silicon-based SiN waveguide

Figure 7(a)–(h) presents the electric field distributions across the XZ plane at various propagation distances (Y = 2.15 to 3.09 μm) for the hybrid reflector design that combines a planar Ag reflector (500 nm below the waveguide) and a 45° inclined Ag reflector. The observed field profiles demonstrate clear multi-mode interference effects within the SiN waveguide, accompanied by periodic power redistribution and lateral mode beating. Compared to previous designs, this configuration exhibits

enhanced field confinement and directional guidance. As shown in Figure 7(i), the planar Ag reflector effectively suppresses out-of-plane radiation by reflecting downward-leaking light back into the waveguide core. Simultaneously, the 45° inclined reflector redirects leftward-propagating light into the forward direction, leading to directional field enhancement. Figure 7(j) confirms that most of the guided light is efficiently funneled toward the output side of the waveguide, minimizing energy loss at the input side. As discussed earlier in Section II, light propagation in the waveguide is primarily affected by two loss pathways: vertical leakage into the SiO$_2$ substrate and backward propagation. The dual-reflector configuration is designed to address both. While the planar reflector efficiently reflects vertically emitted radiation, the 45° inclined reflector plays a dual role by suppressing backward-propagating light and partially redirecting downward

Figure 7

Electronic field distribution with an Ag planar reflector positioned 500 nm from the lower surface of the waveguide and a 45° inclined Ag reflector is shown: where (a) Y = 2.15 µm, (b) Y = 2.27 µm, (c) Y = 2.47 µm, (d) Y = 2.63 µm, (e) Y = 2.76 µm, (f) Y = 2.87 µm, (g) Y = 2.99 µm, (h) Y = 3.09 µm. The cross-sectional energy distribution of the design at the central position is shown in the (i) XZ plane and in the (j) YZ plane; (k) the transmission efficiency and average coupling efficiency for the design featuring a 45° inclined Ag reflector and an Ag planar reflector, positioned 500 nm from the lower surface of the waveguide are shown
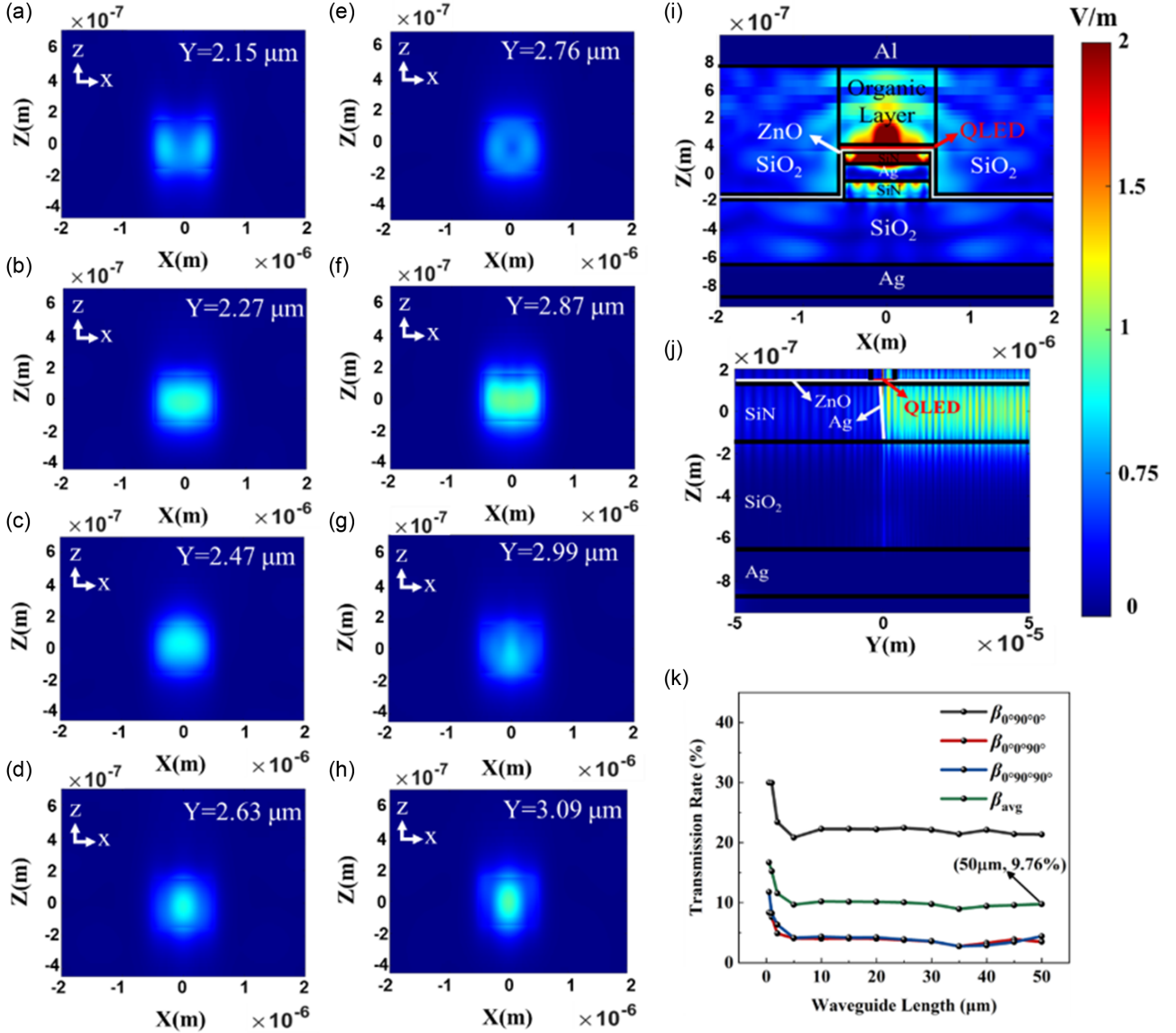
leakage. Although this vertical suppression effect is less visually apparent in Figure 6(j), a direct comparison between the dual-reflector configuration (Figure 7(j)) and the single planar reflector case (Figure 4(j)) reveals notable attenuation of downward leakage in both the central and left regions. This observation suggests that the 45° reflector not only redirects backward-guided modes toward the output but also intercepts vertical emission and prevents energy escape into the substrate. As a result, the incremental benefit of combining both reflectors is reduced due to partial functional overlap, explaining why the average coupling efficiency improvement from the dual-reflector design is modest relative to the single inclined reflector. Figure 7(k) illustrates the transmission efficiency trends for dipole sources oscillating along

the X, Y, and Z directions. The transmission curves stabilize after 10 µm, and the average coupling efficiency β_{avg} reaches 9.76% at 50 µm from the waveguide center. This represents a 2.58 times improvement over the basic design (β_{avg} = 3.78%) and slightly exceeds the performance of the inclined-only configuration. These results demonstrate that the combined reflector structure effectively enhances vertical confinement and directional recoupling, ultimately yielding the highest waveguide output efficiency among all evaluated designs. For the experiment, many issues such as electrical and thermal management, interface defects need to be considered. In addition to assessing the robustness of the proposed coupling design under realistic fabrication conditions, we conducted a tolerance analysis focusing

on reflector placement deviations and etching angle variations. The results, presented in Figure A1, demonstrate that the reflector-assisted configuration maintains superior coupling efficiency compared to the baseline design across a practical range of deviations. This confirms the feasibility of the proposed scheme for experimental implementation. Furthermore, considering the practical QD layer thickness and potential positional deviations due to fabrication, we performed a dipole position tolerance analysis within the xy-plane. The results, shown in Figure A2 of the Appendix, indicate that variations in dipole position have a limited impact on the average coupling efficiency, thereby confirming the robustness of the design against spatial non-uniformities in the QD emissive layer.

4. Conclusion

In summary, this work proposed a design of on-chip CdSe/CdS QD-LED coupled with SiN waveguide on Si substrate. However, the basic design has two main light loss paths: one is the light transmitted into the SiO_2, and the other one is the light transmitted in the opposite direction of the output energy. In order to improve the average coupling efficiency, for the first light loss path, an Ag planar reflector is introduced below the SiN waveguide to reflect the light transmitted into the SiO_2 back into the waveguide. For the second light loss path, the design introduces an inclined Ag reflector within the SiN waveguide directly below the coupled light source to reflect light transmitted in the opposite direction of the output energy back to the energy output end. In the optimization simulation, the QDs are approximated as point dipole sources, and the dipole model is used for optical simulation. The simulation results show that, for the Ag planar reflector, the position from the lower surface of the waveguide ranges from 0 to 700 nm, with the average transmission efficiency being optimal at 500 nm. The average transmission efficiency β_{avg} of the design with an Ag planar reflector at 500 nm is 8.76%, compared with the basic design increased to over 2.32 times. As for the inclined Ag reflector, the angle ranges from 40° to 49°, with the average transmission efficiency being optimal at 45°. The average transmission efficiency β_{avg} of the design with a 45° inclined Ag reflector is 9.39%, compared with the basic design increased to over 2.48 times. Moreover, the optimized design is built to include both an Ag planar reflector at 500 nm and a 45° inclined Ag reflector, and the average transmission efficiency β_{avg} is 9.76%. Compared with the basic design, the average transmission efficiency β_{avg} is increased to over 2.58 times. This research confirms the positive effect of Ag reflector in the coupling efficiency of CdSe/CdS QDs on silicon substrates as on-chip light sources directly coupled to SiN waveguide, providing a feasible scheme for directly coupling a high-efficiency light source with a waveguide on a silicon substrate.

Funding Support

Ethical Statement

This study does not contain any studies with human or animal subjects performed by any of the authors.

Conflicts of Interest

The authors declare that they have no conflicts of interest to this work.

Data Availability Statement

Data are available from the corresponding author upon reasonable request.

Author Contribution Statement

Jiajun Zhu: Validation, Formal analysis, Investigation, Data curation, Writing – original draft, Writing – review & editing, Visualization. **Yuxuan Ye:** Software, Validation, Data curation, Writing – original draft, Writing – review & editing. **Fankai Zheng:** Software, Validation, Investigation. **Yilan Zhang:** Writing – review & editing, Visualization. **Zhiyang Lu:** Software, Writing – review & editing. **Hechun Zhang:** Data curation, Writing – review & editing. **Sifan Chen:** Writing – review & editing, Supervision. **Jiongwen Fang:** Writing – review & editing. **Yunji Yi:** Methodology, Resources, Writing – review & editing, Supervision. **Kai Wang:** Methodology, Resources, Writing – review & editing, Supervision. **Dan Wu:** Conceptualization, Methodology, Resources, Writing – review & editing, Supervision, Project administration, Funding acquisition.

References

[1] Nagarajan, R., Joyner, C. H., Schneider, R. P., Bostak, J. S., Butrie, T., Dentai, A. G., . . . , & Welch, D. F. (2005). Large-scale photonic integrated circuits. *IEEE Journal of Selected Topics in Quantum Electronics*, *11*(1), 50–65. https://doi.org/10.1109/JSTQE.2004.841721

[2] Zhang, J., Shankar, A. G., & Wang, X. (2024). On-chip lasers for silicon photonics. *Photonics*, *11*(3), 212. https://doi.org/10.3390/photonics11030212

[3] Hansel, A., & Heck, M. J. R. (2020). Widely tunable laser on an InP photonic integrated circuit. *IEEE Photonics Technology Letters*, *32*(2), 105–108. https://doi.org/10.1109/LPT.2019.2958711

[4] Tough, E. J., Fice, M. J., Renaud, C. C., Seddon, J., Seeds, A. J., Graham, C., Balakier, K., & Carpintero, G. (2021). InP photonic integrated circuit for 6.7GHz spaced optical frequency comb generator. In *2021 International Topical Meeting on Microwave Photonics*, 1–4. https://doi.org/10.1109/MWP53341.2021.9639427

[5] Rogers, C., Piggott, A. Y., Thomson, D. J., Wiser, R. F., Opris, I. E., Fortune, S. A., . . . , & Nicolaescu, R. (2021). A universal 3D imaging sensor on a silicon photonics platform. *Nature*, *590*(7845), 256–261. https://doi.org/10.1038/s41586-021-03259-y

[6] Xiang, C., Liu, J., Guo, J., Chang, L., Wang, R. N., Weng, W., . . . , & Bowers, J. E. (2021). Laser soliton microcombs heterogeneously integrated on silicon. *Science*, *373*(6550), 99–103. https://doi.org/10.1126/science.abh2076

[7] Lischke, S., Peczek, A., Morgan, J. S., Sun, K., Steckler, D., Yamamoto, Y., . . . , & Zimmermann, L. (2022). Ultra-fast germanium photodiode with 3-dB bandwidth of 265 GHz.

Nature Photonics, *16*(3), 258. https://doi.org/10.1038/s41566-021-00948-y

[8] Du, Y., Jiang, H., Zhu, B., Yan, H., Chai, Y., Tsoi, C. C., . . . , & Wang, C. (2025). A universal bonding strategy for achieving CMOS-compatible silicon heterogeneous integration. *Advanced Materials Technologies*. Advance online publication. https://doi.org/10.1002/admt.202402063

[9] Zhou, Z., Ou, X., Fang, Y., Alkhazraji, E., Xu, R., Wan, Y., & Bowers, J. E. (2023). Prospects and applications of on-chip lasers. *eLight*, *3*(1), 1. https://doi.org/10.1186/s43593-022-00027-x

[10] Adcock, J. C., Bao, J., Chi, Y., Chen, X., Bacco, D., Gong, Q., . . . , & Ding, Y. (2021). Advances in silicon quantum photonics. *IEEE Journal of Selected Topics in Quantum Electronics*, *27*(2), 6700224. https://doi.org/10.1109/JSTQE.2020.3025737

[11] Pérez, D., Gasulla, I., Crudgington, L., Thomson, D. J., Khokhar, A. Z., Li, K., . . . , & Capmany, J. (2017). Multipurpose silicon photonics signal processor core. *Nature Communications*, *8*(1), 1925. https://doi.org/10.1038/s41467-017-01529-w

[12] Izhaky, N., Morse, M. T., Koehl, S., Cohen, O., Rubin, D., Barkai, A., . . . , & Paniccia, M. J. (2006). Development of CMOS-compatible integrated silicon photonics devices. *IEEE Journal of Selected Topics in Quantum Electronics*, *12*(6), 1688–1698. https://doi.org/10.1109/JSTQE.2006.884089

[13] Lee, Y. H. D., & Lipson, M. (2013). Back-end deposited silicon photonics for monolithic integration on CMOS. *IEEE Journal of Selected Topics in Quantum Electronics*, *19*(2), 8200207. https://doi.org/10.1109/JSTQE.2012.2209865

[14] Shi, Y., Zhang, Y., Wan, Y., Yu, Y., Zhang, Y., Hu, X., . . . , & Pan, B. (2022). Silicon photonics for high-capacity data communications. *Photonics Research*, *10*(9), A106–A134. https://doi.org/10.1364/PRJ.456772

[15] Dong, P., Chen, Y.-K., Duan, G.-H., & Neilson, D. T. (2014). Silicon photonic devices and integrated circuits. *Nanophotonics*, *3*(4–5), 215–228. https://doi.org/10.1515/nanoph-2013-0023

[16] Zhang, Z., Zhang, S., Liu, X., Wei, Z., Sharma, T., Murugan, G. S., . . . , & Cheng, Z. (2025). Integrated optical spectrometers on silicon photonics platforms. *Laser & Photonics Reviews*, *19*(7), 2400155. https://doi.org/10.1002/lpor.202400155

[17] Soref, R., Shastri, B. J., & Tait, A. N. (2023). The silicon-based XOI wafer: The most general electronics-photonics platform for computing, sensing, and communications. *IEEE Journal of Selected Topics in Quantum Electronics*, *29*(2), 8200108. https://doi.org/10.1109/jstqe.2022.3211310

[18] Sun, X., Zadok, A., Shearn, M. J., Diest, K. A., Ghaffari, A., Atwater, H. A., . . . , & Yariv, A. (2009). Electrically pumped hybrid evanescent Si/InGaAsP lasers. *Optics Letters*, *34*(9), 1345–1347. https://doi.org/10.1364/OL.34.001345

[19] Xiang, C., Guo, J., Jin, W., Wu, L., Peters, J., Xie, W., . . . , & Bowers, J. E. (2021). High-performance lasers for fully integrated silicon nitride photonics. *Nature Communications*, *12*(1), 6650. https://doi.org/10.1038/s41467-021-26804-9

[20] Wei, W.-Q., He, A., Yang, B., Wang, Z.-H., Huang, J.-Z., Han, D., . . . , & Wang, T. (2023). Monolithic integration of embedded III–V lasers on SOI. *Light: Science & Applications*, *12*(1), 84. https://doi.org/10.1038/s41377-023-01128-z

[21] Wang, J., & Long, Y. (2018). On-chip silicon photonic signaling and processing: A review. *Science Bulletin*, *63*(19), 1267–1310. https://doi.org/10.1016/j.scib.2018.05.038

[22] Park, M., Song, J., An, M., Lim, J., Lee, C., Roh, J., & Lee, D. (2020). Colloidal quantum dot light-emitting diodes employing solution-processable tin dioxide nanoparticles in an electron transport layer. *RSC Advances*, *10*(14), 8261–8265. https://doi.org/10.1039/D0RA00653J

[23] Shan, Q., Dong, Y., Xiang, H., Yan, D., Hu, T., Yuan, B., . . . , & Zeng, H. (2024). Perovskite quantum dots for the next-generation displays: Progress and prospect. *Advanced Functional Materials*, *34*(36), 2401284. https://doi.org/10.1002/adfm.202401284

[24] Hu, H., Levchuk, I., Kalkowski, F., Elia, J., Osvet, A., & Brabec, C. J. (2023). Engineering stable perovskite film for high color purity display application. *ACS Energy Letters*, *8*(10), 4380–4385. https://doi.org/10.1021/acsenergylett.3c01812

[25] Tian, D., Ma, H., Huang, G., Gao, M., Cai, F., Fang, Y., . . . , & Du, Z. (2023). A review on quantum dot light-emitting diodes: From materials to applications. *Advanced Optical Materials*, *11*(2), 2201965. https://doi.org/10.1002/adom.202201965

[26] García de Arquer, F. P., Talapin, D. V., Klimov, V. I., Arakawa, Y., Bayer, M., & Sargent, E. H. (2021). Semiconductor quantum dots: Technological progress and future challenges. *Science*, *373*(6555), eaaz8541. https://doi.org/10.1126/science.aaz8541

[27] Kim, J., Roh, J., Park, M., & Lee, C. (2024). Recent advances and challenges of colloidal quantum dot light-emitting diodes for display applications. *Advanced Materials*, *36*(20), 2212220. https://doi.org/10.1002/adma.202212220

[28] Khadka, S. (2014). *Colloidal quantum dot based light emitting devices on silicon substrate.* Master's Thesis, University of Illinois.

[29] Kim, L., Anikeeva, P. O., Coe-Sullivan, S. A., Steckel, J. S., Bawendi, M. G., & Bulović, V. (2008). Contact printing of quantum dot light-emitting devices. *Nano Letters*, *8*(12), 4513–4517. https://doi.org/10.1021/nl8025218

[30] Elsinger, L., Petit, R., van Acker, F., Zawacka, N. K., Tanghe, I., Neyts, K., . . . , & van Thourhout, D. (2021). Waveguide-coupled colloidal quantum dot light emitting diodes and detectors on a silicon nitride platform. *Laser & Photonics Reviews*, *15*(7), 2000230. https://doi.org/10.1002/lpor.202000230

[31] Ussembayev, Y. Y., Hens, Z., & Neyts, K. (2019). Contrasting anisotropy of light absorption and emission by semiconductor nanoparticles. *ACS Photonics*, *6*(5), 1146–1152. https://doi.org/10.1021/acsphotonics.8b01405

[32] Zhang, Z., Chen, X., Cheng, Q., Khokhar, A. Z., Yan, X., Huang, B., . . . , & Reed, G. T. (2019). High-efficiency apodized bidirectional grating coupler for perfectly vertical coupling. *Optics Letters*, *44*(20), 5081–5084. https://doi.org/10.1364/OL.44.005081

[33] Huang, W.-T., Hong, K.-B., Liu, A.-C., Wang, H.-C., Lin, C.-H., Weng, C.-Y., . . . , & Kuo, H.-C. (2025). Designing an efficient silicon photonics system: Direct integrating photonic crystal surface emitting laser with inverse-designed perfect vertical grating coupler for optimal optical communication applications. *Journal of Lightwave Technology*, *43*(7), 3338–3347. https://doi.org/10.1109/JLT.2024.3522087

[34] Schnauber, P., Singh, A., Schall, J., Park, S. I., Song, J. D., Rodt, S., . . . , & Davanco, M. (2019). Indistinguishable photons from deterministically integrated single quantum dots in heterogeneous GaAs/Si$_3$N$_4$ quantum photonic circuits. *Nano Letters*, *19*(10), 7164–7172. https://doi.org/10.1021/acs.nanolett.9b02758

[35] Pholsen, N., Ota, Y., & Iwamoto, S. (2024). Design of GaAs microcavity on SiN waveguide for efficient single-photon generation by resonant excitation. *Materials for Quantum Technology*, *4*(2), 026201. https://doi.org/10.1088/2633-4356/ad4e8c

[36] Blau, Y., Gilad, T., Hanein, Y., Boag, A., & Scheuer, J. (2022). High efficiency coupling to metal-insulator-metal plasmonic waveguides. *Optics Express*, *30*(8), 13757–13764. https://doi.org/10.1364/OE.453240

[37] Wang, Y., Zhang, F., Yan, C., Gao, R., & Guo, S. (2017). SiO_2/Ag/SiO_2 sān céng jiégòu zhìbèi jí qí SERS xìngnéng de yánjiū [Preparation of SiO_2/Ag/SiO_2 sandwich structure for SERS study]. *Journal of Jilin Normal University: Natural Science Edition*, *38*(4), 20–24. https://doi.org/10.16862/j.cnki.issn1674-3873.2017.04.004

[38] Nyknen, H., Drake, J. P., Kho, E., Lerose, D., Mkel, S. L., & Nagra, A. S. (2020). *Waveguide mirror and method of fabricating a waveguide mirror* (U.S. Patent No. US10641962B2). Google Patents. https://patents.google.com/patent/US10641962B2/en

[39] Beane, G., Boldt, K., Kirkwood, N., & Mulvaney, P. (2014). Energy transfer between quantum dots and conjugated dye molecules. *The Journal of Physical Chemistry C*, *118*(31), 18079–18086. https://doi.org/10.1021/jp502033d

[40] Guzmán-Sepúlveda, J. R., Guzmán-Cabrera, R., & Castillo-Guzmán, A. A. (2021). Optical sensing using fiber-optic multimode interference devices: A review of nonconventional sensing schemes. *Sensors*, *21*(5), 1862. https://doi.org/10.3390/s21051862

[41] Chen, M., Lu, L., Yu, H., Li, C., & Zhao, N. (2021). Integration of colloidal quantum dots with photonic structures for optoelectronic and optical devices. *Advanced Science*, *8*(18), 2101560. https://doi.org/10.1002/advs.202101560

Appendix

Figure A1
Analysis of the impact of fabrication-related variations on waveguide coupling efficiency is shown: (a) the average coupling efficiency of different Ag planar reflector positions relative to the lower surface of the waveguide and (b) the average coupling efficiency of different angles of inclined Ag reflector
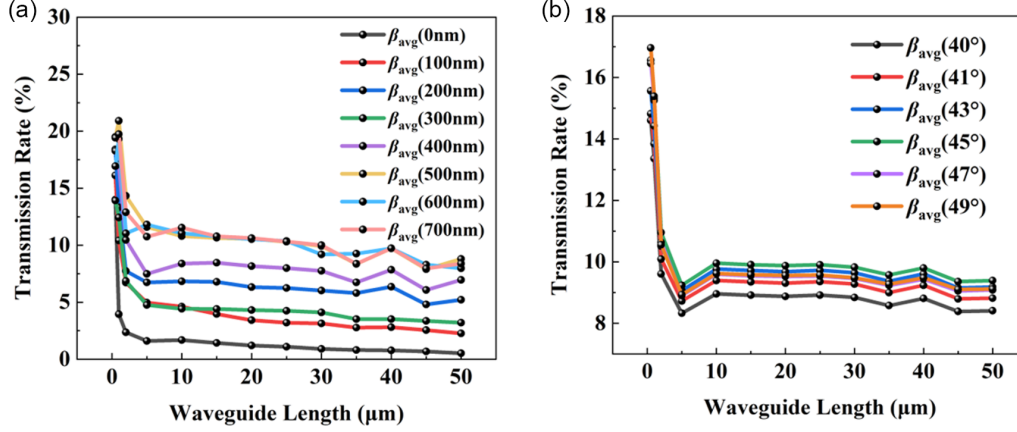
Figure A2
Analysis of the impact of dipole source position deviations in the XY plane on waveguide coupling efficiency, based on the basic design without Ag reflectors: (a) average coupling efficiency for dipoles shifted along the X-axis, and (b) average coupling efficiency for dipoles shifted along the Y-axis. The Y-axis corresponds to the long axis and the X-axis to the short axis of the structure, with the positive Y direction pointing toward the waveguide output